A wireless, implantable optoelectrochemical probe for optogenetic stimulation and dopamine detection

Changbo Liu,[1] Yu Zhao,[2] Xue Cai,[2] Yang Xie,[2] Taoyi Wang,[3] Dali Cheng,[2] Lizhu Li,[2] Rongfeng Li,[4] Yuping Deng,[5] He Ding,[6] Guoqing Lv,[6] Guanlei Zhao,[7] Lei Liu,[7] Guisheng Zou,[7] Meixin Feng,[8] Qian Sun,[8] Lan Yin,[5] Xing Sheng[2, *]

Affiliations

[1]School of Materials Science and Engineering, Beihang University, Beijing, 100191, China

[2]Department of Electronic Engineering, Beijing National Research Center for Information Science and Technology and IDG/McGovern Institute for Brain Research, Tsinghua University, Beijing, 100084, China

[3]Department of Physics, Tsinghua University, Beijing, 100084, China

[4]Beijing Institute of Collaborative Innovation, Beijing, 100094, China

[5]School of Materials Science and Engineering, Tsinghua University, Beijing, 100084 China

[6]School of Optics and Photonics, Beijing Institute of Technology, Beijing, 100081, China

[7]Department of Mechanical Engineering, Tsinghua University, Beijing, 100084, China

[8]Key Laboratory of Nano-devices and Applications, Suzhou Institute of Nano-Tech and Nano-Bionics, Chinese Academy of Sciences (CAS), Suzhou 215123, China

*Correspondence to: xingsheng@tsinghua.edu.cn

ABSTRACT

Physical and chemical technologies have been continuously progressing advances of neuroscience research. The development of research tools for closed-loop control and monitoring neural activities in behaving animals is highly desirable. In this paper, we introduce a wirelessly operated, miniaturized microprobe system for optical interrogation and neurochemical sensing in the deep brain. Via epitaxial liftoff and transfer printing, microscale light emitting diodes (micro-LEDs) as light sources, and poly(3,4-ethylenedioxythiophene) polystyrene sulfonate (PEDOT:PSS) coated diamond films as electrochemical sensors are vertically assembled to form implantable optoelectrochemical probes, for real-time optogenetic stimulation and dopamine detection capabilities. A customized, lightweight circuit module is employed for untethered, remote signal control and data acquisition. Injected into the ventral tegmental area (VTA) of freely behaving mice, *in vivo* experiments clearly demonstrate the utilities of the multifunctional optoelectrochemical microprobe system for optogenetic interference of place preferences and detection of dopamine release. The presented options for material and device integrations provide a practical route to simultaneous optical control and electrochemical sensing of complex nervous systems.

INTRODUCTION

In the past decades, the study of modern neuroscience has been significantly advanced, along with the monumental progresses of interdisciplinary technological innovations in fields including electrophysiology[1], optical interrogation/detection[2] and neuropharmacology[3]. Although traditional electrical tools for neural recording and medication provide powerful capabilities for brain science research and clinical therapies of neurological disorders like Parkinson's disease and epilepsy[4], the lack of cell-type specificity and side effects of stimulating untargeted brain regions impede their broader applications[5]. Recently developed genetically encoded optical actuators and indicators overcome the above limitations and offer more precise and cell specific neural signal regulation and monitoring[6, 7]. Additionally, multifunctional optical neural interfaces, comprising highly integrated, implantable microscale optoelectronic and microfluidic devices, have achieved remarkable accomplishments in optical/electrical/chemical multimodal sensing and modulation in the deep brain[8-10]. Representative examples include our recently developed optoelectronic probes for wireless optogenetic stimulation and fluorescence recording in freely moving rodents[11-15]. Besides electrical pulses and calcium flows, neurotransmitters, which comprise a plethora of chemicals like dopamine, glutamate, serotonin, etc., are of critical importance and direct relevance in neural activities and brain functions[16, 17]. Among the family of neurotransmitters, dopamine arouses particular interests because of its tight association with important behaviors like motivation, reward, and reinforcement[18]. Therefore, it is highly desirable to develop a fully integrated

implantable system leveraging optogenetic stimulators and dopamine sensors for closed-loop neural stimulation and recording. A commonly used method for dopamine detection involves tethered electrochemical probes made of carbon or noble metals like gold and platinum, which could potentially be bundled with optical fibers for optical simulation[19-21]. More recently, genetically encoded fluorescence indicators of various neurotransmitters have also been actively exploited[22-25]. Integrating the detection of neurotransmitter levels within the wirelessly operated optogenetic stimulation platforms in living animals, however, is relatively underexplored in state-of-the-art studies.

In this paper, we develop a wireless thin-film based implantable microprobe system for optogenetic stimulation and electrochemical sensing of dopamine in the animal deep brain. A thin-film, microscale light-emitting diode (micro-LED) transferred on a flexible substrate is employed as a light source for optogenetic stimulation. A poly(3,4-ethylenedioxythiophene) polystyrene sulfonate (PEDOT:PSS) coated diamond film is placed upon the micro-LED, serving as an electrochemical sensor for dopamine detection. As an optically transparent, electrically insulating and thermally conductive interlayer in the stacked device structure, the diamond film separates the micro-LED and the PEDOT:PSS sensor, ensuring simultaneous optical stimulation and electrochemical detection in the same region. For wireless control and signal acquisition, the formed thin-film and flexible microprobe is interfaced with a miniaturized, removable circuit module powered by a rechargeable battery. Implanted

into the ventral tegmental area (VTA) of freely behaving mice, the fully integrated optoelectrochemical microprobe is demonstrated to remotely control animal behaviors and dopamine signal recording.

RESULTS AND DISCUSSION

Device structure, fabrication and functionality

Fig. 1a schematically displays the conceptual illustration of our proposed implantable, fully integrated microprobe system for simultaneous optogenetic stimulation and electrochemical sensing in the deep brain tissue, with an exploded view shown in Fig. 1b. From bottom to top, the thin-film device stack incorporates a flexible double side copper (Cu) coated polyimide (PI) (18 μm Cu / 25 μm PI / 18 μm Cu) substrate, an indium gallium nitride (InGaN) based blue emitting micro-LED (size: 125 μm × 185 μm × 7 μm), an undoped diamond interlayer (size: 180 μm × 240 μm × 20 μm) and a PEDOT:PSS film (size: 150 μm × 200 μm × 0.1 μm). The emission from the blue LED is utilized to optogenetically control specific cells expressing light-sensitive ion channels, for example, channelrhodopsin-2 (ChR2) [6, 7, 26-28], thereby activating or inhibiting neural activities. As an optically transparent and electrically conductive polymer layer, the PEDOT:PSS thin film can work as an effective electrochemical sensor for dopamine detection, owing to its biocompatibility and low impedance at the biological interface[29-32]. As an interlayer between the LED and the PEDOT:PSS sensor, the benefits of using the diamond film are manifold: 1) Its optical transparency (> 80%)[33] ensures that the blue light can transmit through it

and reach the bio-tissue; 2) Its high thermal conductivity (> 2000 W/m/K)[34] allows for efficient heat dissipation during LED operation; 3) It electrically isolates the electrodes of the LED and the PEDOT:PSS film, minimizing signal crosstalk; and 4) It could act as a liquid barrier and prevent the LED from failure in aqueous environment. The LED is fabricated on sapphire and the diamond film is grown on silicon. They are released from native substrates respectively by laser liftoff and wet etching, forming freestanding films transferred onto PI using polydimethylsiloxane (PDMS) stamping methods[35, 36]. On the diamond layer, the PEDOT:PSS film is conformally coated via spin casting and lithographically patterned, with a thickness of ~100 nm (Fig. 1c). The LED and PEDOT:PSS film are metalized with deposited gold electrodes, while epoxy-based photoresist films (SU-8) serve as the bonding layer between the LED and the diamond, as well as the protective coating on metal electrodes. Finally, the flexible substrate is milled by ultraviolet laser to realize a needle shape (width ~ 360 μm, length ~ 5 mm, shown in Fig. 1d), which is ready for implantation into the deep tissue of animal brains. Compared with other possible device geometries like physically bonded fibers/wires[37, 38] or laterally placed thin-film sensors[14, 39, 40], the vertically stacked device structure is more advantageous because: 1) It has a higher spatial precision in the control and the monitoring of a specifically targeted nucleus, which typically have sizes from tens to hundreds of micrometers in the mouse brain; and 2) Such a thin-film geometry can have a smaller footprint and desirable mechanical flexibility, significantly reducing tissue lesion and associated damages.

Optoelectronic and thermal properties

The utility of freestanding InGaN based micro-LEDs for optogenetic stimulations has been demonstrated in previous works[36]. Here we evaluate optical and thermal properties of the micro-LED before and after integrating with the PEDOT:PSS coated diamond film for electrochemical sensing, with results depicted in Fig. 2. Under current injection, the peak wavelength for the LED emission is around 470 nm (Fig. 2a), which matches to the optical absorption of commonly used opsins like ChR2 as optogenetic tools[13, 26-28]. The external quantum efficiency (EQE) for LEDs with and without diamond and PEDOT:PSS films are plotted in Fig. 2b. Maximum EQEs are ~12% (for the bare LED) and ~10% (for the LED coated with diamond and PEDOT:PSS), obtained at an injection current of ~1 mA. In addition, both devices exhibit nearly Lambertion emission distributions (Fig. 2c). These results indicate that the diamond/PEDOT:PSS film placed on top of the blue LED does not greatly alter its emission characteristics, and the slight performance degradation (~20%) is in accordance with the optical transmission of the diamond and the PEDOT:PSS materials (>80%)[33, 41].

Besides optical transparency, another prominent feature of the diamond film is its ultrahigh thermal conductivity. Even through the diamond film we apply here has a polycrystalline morphology, its thermal conductivity still reaches as high as 2200 W/m/K, almost 5 times higher than copper films and 3 orders of magnitude higher

than organic coatings like SU-8 and PDMS[42]. Such a thermally conductive coating is advantageous for heat dissipation of LEDs operated in biological systems. In Fig. 2d–f, we evaluate the thermal behaviors for LEDs with and without diamond/PEDOT:PSS coatings. The LEDs are operated in ambient air under pulsed current injection (varied from 0 to 10 mA), with 20 Hz frequency and 20% duty cycle. Temperature maps are measured with an infrared camera and compared with thermal modeling established by finite element analysis. As shown in Fig. 2d, the maximum temperature rises for the LED with diamond are approximately one half of those for the bared LED under the same injection currents. Thermal mapping results for LEDs operated at 3 mA are further depicted in Fig. 2e and 2f. These experimental results are in good agreement with numerical predictions. At 3 mA, the probe surface temperature increase is restricted within 2 °C for the LED with the diamond coating, while the result for the bare LED is more than 4 °C. Furthermore, it should be noted that for the microprobe implanted in biological tissues, the temperature rises, albeit more challenging to measure precisely, should be even lower than the results obtained in air, because of the additional heat dissipation capability of biological tissues and fluids. This benefit is particularly favorable for optogenetic probes implanted in the deep brain, since the mitigation of unwanted abnormal activities and possible tissue damaging by overheating is critical for neurons [43].

Electrochemical characterization

Electrochemical properties of the PEDOT:PSS electrode for dopamine sensing are

studied and presented in Fig. 3. The detection of dopamine in aqueous solutions is based on its redox reaction, in which dopamine is oxidized and converted into dopamine-o-quinone on the electrode surface, generating electric currents[44]. Cyclic voltammetry (CV), differential pulse voltammetry (DPV), chronoamperometry (CA), and fast scan cyclic voltammetry (FSCV) techniques are utilized to analyze the electrochemical features of PEDOT:PSS electrode, using a standard electrochemical work station. A standard three-electrode configuration is applied, with the PEDOT:PSS film serving as the working electrode (WE), silver/silver chloride (Ag/AgCl) and platinum (Pt) as the reference (RE) and the counter electrodes (CE), respectively. Here we use dilute hydrochloric acid (HCl) solutions (pH = 4.0) as solvents for dopamine, in order to mitigate its degradation due to natural oxidation in air that causes measurement inaccuracy[45, 46]. As the CV results shown in Fig. 3a, a pair of well-defined quasi-reversible redox peaks are observed in the presence of dopamine in HCl, with oxidation potentials of 0.5–0.6 V and the corresponding reduction potentials of 0.3–0.4 V. Peak redox currents increase with the concentration of dopamine in the solution. DPV measurements in Fig. 3b reveal similar trends, with a higher sensitivity of concentration and a better voltage resolution than those obtained with CV analysis. Dopamine levels in HCl solutions as low as ~0.1 μM can be detected using DPV. The dynamic current response at varied dopamine concentrations is further determined using CA measurements in Fig. 3c and 3d. At a fixed bias voltage of 0.6 V, oxidation currents are captured as we change dopamine concentrations. In the range of 0.1–10 μM, a linear relationship between the dopamine

concentration and the response current can be obtained, and the detection sensitivity is determined to be ~0.06 nA/μM. For our spin coated PEDOT:PSS film, the normalized current response of dopamine by area is calculated to be 200 nA/μM/cm^2, which is comparable to that measured by electrochemical sensors based on other materials[47, 48]. In Fig. 3e, we further record the FSCV responses by dropping dopamine solutions in HCl, plotting the current response as a function of both time and voltage. It should be noted that CV, DPV, CA and FSCV measurements exhibit different current sensitvities at varied dopamine concentrations, because part of the measured electrochemical currents are associated with the capacity at the electrode/electrolyte interface, which is highly sensentive to the applied applying different potential modulation forms and scan rates[49]. The experimental results performed *in vitro* clearly demonstrate the utility of applying the PEDOT:PSS film for real-time dopamine monitoring in biological systems.

Circuit design and evaluation

A customized circuit module is designed to wirelessly operate the implantable microprobe for integrated optoelectrochemical stimulation and sensing functionalities. The circuit diagram is depicted in Fig. 4a, with detailed layout presented in the supplemental information. Remote data communication is realized with a micro controller (nRF24LE1) with a transceiver operated at 2.4 GHz. A driver chip (ZLED7012) provides a constant current to the micro-LED for optogenetic stimulation, with programmable current levels, frequencies, pulse widths, etc. A red

LED is printed on the circuit outside the brain for signal indication. A digital-analog converter (DAC60508) and two pre-amplifiers (OPA2381 and ADA4505) are connected to the chemical electrodes (WE, RE and CE) for voltage scanning and current readout, achieving a resolution as low as 0.1 nA for current measurements. The system is powered by a rechargeable lithium ion battery with a capacity of 35 mAh. As shown in Fig. 4b, the microprobe containing a blue micro-LED and a PEDOT:PSS coated diamond film as an electrochemical sensor is connected to the wireless circuit module with a footprint of ~2.2 cm × 1.3 cm and a weight of ~2 g. Via a flexible printed circuit connector, the manufactured circuit can be plugged into the implantable microprobe during *in vivo* experiments and detached from it when unnecessary. The miniaturized wireless module can be easily mounted on the head of an adult mouse, without affecting its behaviors (Fig. 4c). We evaluate the performance of our designed wireless circuit *in vitro* by taking CV scans in HCl solutions with various dopamine concentrations, using a microprobe containing the PEDOT:PSS thin-film electrode. The measured CV results in Fig. 4d match reasonably well with those obtained using a commercial electrochemical analyzer, with clearly resolved redox peaks of dopamine. Similarly, CA measurements (current versus time at a fixed bias voltage) can also be performed. These results demonstrate the utility of the wireless circuit for *in vivo* tests in behaving animals.

***In vivo* experiments**

We further verify the performance of the wirelessly operated microprobe, with *in vivo*

optogenetic stimulation and dopamine sensing in experimental mouse models. Illustrated in Fig. 5a and 5b, probes including micro-LEDs and PEDOT:PSS electrodes are implanted into the ventral tegmental area (VTA), which is the origin of dopaminergic cells and involves reward circuitry[50, 51]. A microprobe with a length of ~5 mm is implanted into the VTA of adult mice (DAT-Cre transgenic, 7–16 weeks) expressing ChR2. Fig. 5b shows a brain section with the lesion area created by the implanted microprobe. Details of the immunostained region in the VTA are provided in Fig. 5c, including stained ChR2 (red), rabbit polyclonal anti-tyrosine hydroxylase (TH, green), 4',6-diamidino-2-phenylindole (DAPI, blue) and merged images. The track of the probe is indicated by the dashed boxes. We perform real-time place preference (RTPP) tests by optogenetic stimulation 5 days after implanting microprobes into the VTA of mice. Results are schematically illustrated in Fig. 5d. Mice are placed in a behavior box (50 cm × 25 cm × 25 cm) with two chambers and a gate with a width of 9 cm (Fig. 5d, upper part). Animals are allowed to explore the environment for 15 minutes to get a pre-test result, and only those with no obvious place preference are used for optogenetic test. After pre-test, optical stimulation (duration: 10 ms, frequency: 20 Hz, driving current: 1.8 mA) generated by the blue-emitting micro-LED is provided for 15 minutes when mices go into the left chamber. The position heatmap (Fig. 5d, lower part) reveals that the mice exhibit obvious place preferences during the optogenetic stimulation period. Statistical results clearly show that animals spend more time in the stimulated chamber compared to pre-tests, indicating that dopaminergic neurons in the VTA are excited and dopamine

release is promoted. As a control group, DAT-Cre mice expressing the AAV-EF1a-DIO-mCherry virus show no obvious place preference under the same light stimulation conditions.

To evaluate the electrochemical sensing capability, we measure CA curves (current versus time) with the PEDOT:PSS electrode implanted in the VTA. Similar to *in vitro* experiments in Fig. 3, here we employ a Ag/AgCl wire and a stainless steel screw respectively as the reference and counter electrodes, which are implanted elsewhere in the mouse brain cortex. A constant forward bias of 0.6 V is applied between the WE and the RE, and the oxidation current flowing into the WE is acquired at an interval of 0.1 s. Fig. 5f plots a representative amperometric results measured with a microprobe implanted into the VTA of mice. Spontaneous current spikes are observed, and more signal traces are analyzed in Fig. 5g from 3 mices. The data collected from multiple individual trials reveal considerable consistency, with time constants matched to dopamine signals reported in other literatures[52-54].

Conclusion

In summary, we report a wirelessly operated microprobe system for neural interrogation and neurotransmitter monitoring in the deep brain. Ultraminiaturized, vertically stacked micro-LED, diamond and PEDOT:PSS films are combined to realize optogenetic stimulation and dopamine sensing in a minimally invasive platform. The unique electrical, optical and thermal properties of the PEDOT:PSS

coated diamond film make the device suitable for highly sensitive electrochemical sensing, without affecting the micro-LED operation. A lightweight, remotely control circuit allows for behavior studies on freely moving mice. In the future, more sophisticated *in vivo* experiments can be performed to demonstrate closed-loop operations, for example, modulate light stimulation in response to the change of dopamine levels, or monitor the dopamine release when varying optical emissions. It should be noted that the sensing capability of the PEDOT:PSS electrodes may be interfered during the optical emission due to possible optoelectronic artifacts similar to those reported on other optotrodes[54], and complex algorithms need to be employed to process the electrochemical data. Additionally, multiple microprobes can be implanted into different regions of the brain, exploring function connectivities among distinct units within the nervous system. Considering that various neurotransmitters such as glutamate, serotonin and norepinephrine, existing in the neural system, specificity for dopamine sensing can be further improved by selective coatings like tyrosinase on the PEDOT:PSS[55]. Although here we only demonstrate acute tests in living mice, chronic operation of electrochemical sensors is also a key challenge for complex behavior experiments. Besides optogenetics and electrochemistry, many research tools including fluorescence photometry[14], electrophysiology[56], and microfluidics[57], can be combined in such a platform, to accomplish multimodal electrical-optical-chemical close-loop modulation and detection of neural activities. We envision that these advanced strategies provide a promising route to tackle unresolved challenges in fundamental neuroscience and medical practices.

MATERIALS AND METHODS

Device fabrication

Micro-LEDs: Details for the micro-LED fabrication are described in the previous work[36]. The InGaN-based blue LEDs are epitaxial grown on sapphire substrates using metal-organic chemical vapor deposition (MOCVD) and lithographically formed. The structure (from bottom to top) consisted of a GaN buffer layer, an n-GaN layer, an InGaN/GaN multiple-quantum-well layer, and a p-GaN layer, with a total thickness of about 7.1 μm. The lateral dimension of LED is defined by inductively coupled plasma reactive ion etching (ICP-RIE), with 4 mTorr pressure, 40 sccm Cl_2, 5 sccm BCl_3, 5 sccm Ar, ICP power 450 W, bias power 75 W, and an etch rate of 0.33 μm/min. Freestanding thin-film micro-LEDs (dimension: 180 μm × 125 μm × 7 μm) are formed by laser liftoff (Light Source: the KrF excimer laser at 248 nm, Coherent, Inc., CompexPro110). The optimized power density for the laser is around 0.7 J/cm^2.

Freestanding diamond film: The polycrystalline diamond film (thickness ~ 20 μm) is grown on single crystalline silicon substrates via chemical vapor deposition (CVD). Laser milling (Nd:YVO4 laser, 1064 nm) is used to cut the film into designed patterns (size: 180 μm × 240 μm) and shapes. The silicon substrate is removed using an etchant solution (CH_3COOH : HNO_3 : HF = 5 : 5 : 2 by weight ratio), realizing freestanding diamond films.

Fabrication of the microprobe: Using pre-patterned polydimethylsiloxane (PDMS) (Dow Corning Sylgard 184 kit, 1:10 weight ratio) stamps, the freestanding LEDs are transferred onto flexible double side Cu coated polyimide (18 μm Cu / 25 μm PI / 18 μm Cu, from DuPont) substrates, with a spin-coated adhesive layer. LEDs are encapsulated with 5 μm thick SU-8 (SU8-3005) as an insulating layer. Sputtered layers of 10 nm Cr / 500 nm Cu / 100 nm Au serve as the metalized electrode, and coating 5 μm thick SU-8 (SU8-3005) as an encapsulation layer. The freestanding diamonds are transferred onto micro-LEDs using similar PDMS stamps with 2 μm thick SU-8 (SU8-2002) as an adhesive layer. A 5 μm thick SU-8 (SU8-3005) film is spin coated on the sample, with the surface of the diamond lithographically exposed. Sputtered 5 nm Cr / 500 nm Au films are used as interconnected electrodes for the PEDOT:PSS films. The PEDOT:PSS film is coated on the diamond as the working electrochemical electrode, and patterned by reactive ion etching (RIE) (0.1 Pa pressure, 100 sccm O_2, 5 sccm SF_6, power 100 W for 200 s). Another photoresist film (SU8-3005, 5μm thick) is patterned on the metal electrodes as a waterproof layer. Subsequently, the flexible substrates are patterned to form needle shapes (width ~360 μm, length ~ 5 mm) by UV laser milling.

Device characterization

SEM images are captured by ZEISS Merlin microscope (15 kV). Optical microscopy images are taken by microscope MC-D800U(C). The EQE of micro-LEDs are measured using an integrating sphere (Labsphere Inc.) and a calibrated Si

photodetector. Thermal images are acquired by an infrared camera (FOTRIC 228). LED emission spectra are collected with a spectrometer (Ocean Optics HR2000+). Far-field angular emission profiles of micro-LEDs are captured by a standard Si photodetector (DET36A, Thorlabs). *In vitro* electrochemical tests of dopamine detection are performed with an electrochemical work station (CHI 650E, Shanghai Chenhua Co., Ltd, China). The CV is performed at a sweep rate of 0.1 V/s from 0 V to 1 V. Conditions for the DPV are, voltage step: 4 mV, pulse time: 200 ms, pulse amplitude: 50 mV, and scan rate: 20 mV/s. The CA is employed at a constant bias of 0.6 V. The FSCV is performed with a sweep rate of 50 V/s from 0 V to 1 V for 2000 circles. All of the electrochemical measurements are carried out in a Faraday cage to avoid electromagnetic disturbance from environments.

Thermal Simulation: The simulations of temperature increase on the surface of LED probes (with and without diamond) are performed by steady-state finite element methods in COMSOL Multiphysics®, using the module of Heat Transfer in Solids. The three-dimensional geometric model of the probed is constructed based on the structure described in this paper. The InGaN LED is defined as the heat source, with the input thermal power density (W/m^3) estimated by

$$Q = V \times I \times (1 - \mathrm{EQE}) \times D / V_{\mathrm{LED}}$$

where V and I are measured voltage and current of the LED under continuous current injection conditions, EQE is the external quantum efficiency, D is the duty cycle of LED in experiments (20% in this study) and V_{LED} is the volume of the LED.

Boundary conditions of natural convection to air are applied to all external surfaces of the probe model, in accordance with the experiment setup, and the air temperature is set to 20 °C. The temperature distribution T is calculated by solving the following heat transfer equation:

$$\rho C_p \mathbf{u} \cdot \nabla T + \nabla \cdot \mathbf{q} = Q$$

$$\mathbf{q} = -\kappa \nabla T$$

where ρ is the material mass density, C_p is the heat capacity at constant pressure and κ is the thermal conductivity. A self-adaptive mesh setup is applied on the geometric model. Solutions of temperature are acquired by a stationary fully-coupled solver within the convergence tolerance of 10^{-5} using Newton iteration methods, and the final results of temperature changes are plotted on the external surface of the probe model from top view.

***In vivo* studies**

Stereotaxic surgery: Animal protocols are approved by Animal Care and Use Committee of Tsinghua University and the National Institute of Biological Sciences, Beijing. Adult (7~16 weeks) DAT-Cre transgenic mice (Jackson Laboratory, strain B6.SJL-Slc6a3tm1.1(cre)Bkmn/ J) are used. Mice are group housed at a constant temperature (23±1 °C) and in a 12-h light/12-h dark cycle (lights on 20:00–08:00). Adult DAT-Cre mice are anaesthetized by intraperitoneal injection of 1%

Pentobarbital Sodium (60 mg/kg). A small hole is made by a drill on the skull, and 500 nl virus (AAV2/9-hEF1a-DIO-hChR2(H134R)-mCherry-WPRE-pA) is injected by a glass micropipette using a microsyringe pump (Nanoliter 2000 injector with the Micro4 controller, WPI) into the VTA (stereotaxic coordinates from bregma (mm): anterior-posterior (AP): -3.40, medial-lateral (ML): +/- 0.50, dorsal-ventral (DV): -4.20) at rate of 46 nl min^{-1}. After suturing the wound, mice recover with the virus expressing for 3 weeks, and then the microprobes are implanted into VTA (stereotaxic coordinates from bregma (mm): anterior-posterior (AP): -3.40, medial-lateral (ML): +/- 0.52, dorsal-ventral (DV): -4.50). The dental cement is used to affix the probes. For dopamine detection, a stainless steel screw is used to work as the counter electrode, and a Ag/AgCl wire works as the reference electrode. Both the CE and the RE are implanted elsewhere in the mouse brain cortex.

Immunohistochemistry: Mice are perfused by the phosphate buffered saline (PBS) solution and followed by 4% paraformaldehyde. Mouse brains are post-fixed in the same paraformaldehyde solution overnight and then immersed in 30% sucrose solution for 24 h. The frozen brains are cut into sections with a thickness of 40 μm, and then the sections are washed by PBS and PBST (0.3% Triton X-100 in PBS) and blocked in 3% bovine serum albumin (BSA) in PBST at room temperature for 1 h. The sections are incubated with primary antibodies (rabbit polyclonal Anti-Tyrosine Hydroxylase Antibody, 1:1000) for 24 h at 24 °C, then washed in PBST for 5 times and incubated with secondary antibodies (Goat anti-Rabbit IgG (H+L) Cross-Adsorbed

Secondary Antibody, Alexa Fluor 488, 1:500) for 2 h at room temperature (avoid light), and finally washed the sections in PBS for 3 times. Fluorescent images are scanned with an automated slider scanner (17026728, Zeiss) and a laser scanning microscope (FV3000, Olympus).

Reference

1. Fox, K.C.R., Foster, B.L., Kucyi, A., Daitch, A.L. & Parvizi, J. Intracranial Electrophysiology of the Human Default Network. *Trends in Cognitive Sciences* **22**, 307-324 (2018).
2. Kim, C.K., Adhikari, A. & Deisseroth, K. Integration of optogenetics with complementary methodologies in systems neuroscience. *Nature Reviews Neuroscience* **18**, 222-235 (2017).
3. Kamp, F. *et al.* Effects of sedative drug use on the dopamine system: a systematic review and meta-analysis of in vivo neuroimaging studies. *Neuropsychopharmacology* **44**, 660-667 (2019).
4. Cogan, S.F. Neural Stimulation and Recording Electrodes. *Annual Review of Biomedical Engineering* **10**, 275-309 (2008).
5. Aravanis, A.M. *et al.* An optical neural interface:in vivocontrol of rodent motor cortex with integrated fiberoptic and optogenetic technology. *Journal of Neural Engineering* **4**, S143-S156 (2007).
6. Kampasi, K. *et al.* Dual color optogenetic control of neural populations using low-noise, multishank optoelectrodes. *Microsystems & Nanoengineering* **4**, 10 (2018).
7. Khan, W. *et al.* Inductively coupled, mm-sized, single channel optical neuro-stimulator with intensity enhancer. *Microsystems & Nanoengineering* **5**, 23 (2019).
8. Pashaie, R. *et al.* Optogenetic brain interfaces. *IEEE reviews in biomedical engineering* **7**, 3-30 (2013).
9. Zhang, S. *et al.* Real-time simultaneous recording of electrophysiological activities and dopamine overflow in the deep brain nuclei of a non-human primate with Parkinson's disease using nano-based microelectrode arrays. *Microsystems & Nanoengineering* **4**, 17070 (2018).
10. Fan, B. *et al.* A hybrid neural interface optrode with a polycrystalline diamond heat spreader for optogenetics. *Technology* **4**, 15-22 (2016).
11. Kim, T.-i. *et al.* Injectable, Cellular-Scale Optoelectronics with Applications for Wireless Optogenetics. *Science* **340**, 211-216 (2013).
12. Shin, G. *et al.* Flexible Near-Field Wireless Optoelectronics as Subdermal Implants for Broad Applications in Optogenetics. *Neuron* **93**, 509-521.e503 (2017).
13. Zhao, Y. *et al.* Wirelessly Operated, Implantable Optoelectronic Probes for Optogenetics in Freely Moving Animals. *IEEE Transactions on Electron Devices* **66**, 785-792 (2018).
14. Lu, L. *et al.* Wireless optoelectronic photometers for monitoring neuronal dynamics in the deep brain. *Proceedings of the National Academy of Sciences* **115**, E1374-E1383 (2018).
15. Ding, H. *et al.* Microscale optoelectronic infrared-to-visible upconversion devices and their use as injectable light sources. *Proceedings of the National Academy of Sciences* **115**, 6632-6637 (2018).

16. Trimbuch, T. & Rosenmund, C. Should I stop or should I go? The role of complexin in neurotransmitter release. *Nature Reviews Neuroscience* **17**, 118-125 (2016).
17. Johnson, K.V.A. & Foster, K.R. Why does the microbiome affect behaviour? *Nature Reviews Microbiology* **16**, 647-655 (2018).
18. Berke, J.D. What does dopamine mean? *Nature Neuroscience* **21**, 787-793 (2018).
19. Bass, C.E. *et al.* Optogenetic control of striatal dopamine release in rats. *Journal of Neurochemistry* **114**, 1344-1352 (2010).
20. Chaudhury, D. *et al.* Rapid regulation of depression-related behaviours by control of midbrain dopamine neurons. *Nature* **493**, 532-536 (2013).
21. Tye, K.M. *et al.* Dopamine neurons modulate neural encoding and expression of depression-related behaviour. *Nature* **493**, 537-541 (2013).
22. Jing, M. *et al.* A genetically encoded fluorescent acetylcholine indicator for in vitro and in vivo studies. *Nature Biotechnology* **36**, 726-737 (2018).
23. Marvin, J.S. *et al.* A genetically encoded fluorescent sensor for in vivo imaging of GABA. *Nature Methods* **16**, 763-770 (2019).
24. Feng, J. *et al.* A Genetically Encoded Fluorescent Sensor for Rapid and Specific In Vivo Detection of Norepinephrine. *Neuron* **102**, 745-761.e748 (2019).
25. Sun, F. *et al.* A Genetically Encoded Fluorescent Sensor Enables Rapid and Specific Detection of Dopamine in Flies, Fish, and Mice. *Cell* **174**, 481-496.e419 (2018).
26. Grossman, N. *et al.* Multi-site optical excitation using ChR2 and micro-LED array. *Journal of neural engineering* **7**, 016004 (2010).
27. Iwai, Y., Honda, S., Ozeki, H., Hashimoto, M. & Hirase, H. A simple head-mountable LED device for chronic stimulation of optogenetic molecules in freely moving mice. *Neuroscience research* **70**, 124-127 (2011).
28. Poher, V. *et al.* Micro-LED arrays: a tool for two-dimensional neuron stimulation. *Journal of Physics D: Applied Physics* **41**, 094014 (2008).
29. Vreeland, R.F. *et al.* Biocompatible PEDOT: Nafion composite electrode coatings for selective detection of neurotransmitters in vivo. *Analytical chemistry* **87**, 2600-2607 (2015).
30. Xu, G., Li, B., Cui, X.T., Ling, L. & Luo, X. Electrodeposited conducting polymer PEDOT doped with pure carbon nanotubes for the detection of dopamine in the presence of ascorbic acid. *Sensors and Actuators B: Chemical* **188**, 405-410 (2013).
31. Xu, G., Jarjes, Z.A., Desprez, V., Kilmartin, P.A. & Travas-Sejdic, J. Sensitive, selective, disposable electrochemical dopamine sensor based on PEDOT-modified laser scribed graphene. *Biosensors and Bioelectronics* **107**, 184-191 (2018).
32. Demuru, S. & Deligianni, H. Surface PEDOT: nafion coatings for enhanced dopamine, serotonin and adenosine sensing. *Journal of The Electrochemical Society* **164**, G129-G138 (2017).

33. Walker, J. Optical absorption and luminescence in diamond. *Reports on Progress in Physics* **42**, 1605 (1979).
34. Wei, L., Kuo, P., Thomas, R., Anthony, T. & Banholzer, W. Thermal conductivity of isotopically modified single crystal diamond. *Physical Review Letters* **70**, 3764 (1993).
35. Park, S.-I. *et al.* Printed assemblies of inorganic light-emitting diodes for deformable and semitransparent displays. *science* **325**, 977-981 (2009).
36. Li, L. *et al.* Heterogeneous Integration of Microscale GaN Light‐Emitting Diodes and Their Electrical, Optical, and Thermal Characteristics on Flexible Substrates. *Advanced Materials Technologies* **3**, 1700239 (2018).
37. Witten, I.B. *et al.* Recombinase-driver rat lines: tools, techniques, and optogenetic application to dopamine-mediated reinforcement. *Neuron* **72**, 721-733 (2011).
38. Stauffer, W.R. *et al.* Dopamine neuron-specific optogenetic stimulation in rhesus macaques. *Cell* **166**, 1564-1571. e1566 (2016).
39. Kwon, K.Y., Sirowatka, B., Weber, A. & Li, W. Opto-μECoG array: A hybrid neural interface with transparent μECoG electrode array and integrated LEDs for optogenetics. *IEEE transactions on biomedical circuits and systems* **7**, 593-600 (2013).
40. Yoshimoto, S. *et al.* in 2016 IEEE Biomedical Circuits and Systems Conference (BioCAS) 476-479 (IEEE, 2016).
41. Admassie, S. *et al.* A polymer photodiode using vapour-phase polymerized PEDOT as an anode. *Solar Energy Materials and Solar Cells* **90**, 133-141 (2006).
42. Hartmann, J., Voigt, P. & Reichling, M. Measuring local thermal conductivity in polycrystalline diamond with a high resolution photothermal microscope. *Journal of applied physics* **81**, 2966-2972 (1997).
43. Owen, S.F., Liu, M.H. & Kreitzer, A.C. Thermal constraints on in vivo optogenetic manipulations. *Nature neuroscience* **22**, 1061-1065 (2019).
44. Venton, B.J. & Wightman, R.M. Psychoanalytical Electrochemistry: Dopamine and Behavior. *Analytical Chemistry* **75**, 414 A-421 A (2003).
45. Thorré, K., Pravda, M., Sarre, S., Ebinger, G. & Michotte, Y. New antioxidant mixture for long term stability of serotonin, dopamine and their metabolites in automated microbore liquid chromatography with dual electrochemical detection. *Journal of Chromatography B: Biomedical Sciences and Applications* **694**, 297-303 (1997).
46. Kankaanpää, A., Meririnne, E., Ariniemi, K. & Seppälä, T. Oxalic acid stabilizes dopamine, serotonin, and their metabolites in automated liquid chromatography with electrochemical detection. *Journal of Chromatography B: Biomedical Sciences and Applications* **753**, 413-419 (2001).
47. Taylor, I.M. *et al.* Enhanced dopamine detection sensitivity by PEDOT/graphene oxide coating on in vivo carbon fiber electrodes. *Biosensors and Bioelectronics* **89**, 400-410 (2017).
48. Belaidi, F.S. *et al.* PEDOT-modified integrated microelectrodes for the

detection of ascorbic acid, dopamine and uric acid. *Sensors and Actuators B: Chemical* **214**, 1-9 (2015).

49. Scholz, F. Voltammetric techniques of analysis: the essentials. *ChemTexts* **1**, 17 (2015).
50. Brischoux, F., Chakraborty, S., Brierley, D.I. & Ungless, M.A. Phasic excitation of dopamine neurons in ventral VTA by noxious stimuli. *Proceedings of the national academy of sciences* **106**, 4894-4899 (2009).
51. Beier, K.T. *et al.* Circuit architecture of VTA dopamine neurons revealed by systematic input-output mapping. *Cell* **162**, 622-634 (2015).
52. Lu, Y., Driscoll, N., Ozden, I., Yu, Z. & Nurmikko, A.V. Modulating dopamine release by optogenetics in transgenic mice reveals terminal dopaminergic dynamics. *Neurophotonics* **2**, 031207 (2015).
53. Bass, C.E., Grinevich, V.P., Kulikova, A.D., Bonin, K.D. & Budygin, E.A. Terminal effects of optogenetic stimulation on dopamine dynamics in rat striatum. *Journal of neuroscience methods* **214**, 149-155 (2013).
54. Chiu, W.-T. *et al.* Real-time electrochemical recording of dopamine release under optogenetic stimulation. *PloS one* **9** (2014).
55. Njagi, J., Chernov, M.M., Leiter, J. & Andreescu, S. Amperometric detection of dopamine in vivo with an enzyme based carbon fiber microbiosensor. *Analytical chemistry* **82**, 989-996 (2010).
56. Patel, A.A., McAlinden, N., Mathieson, K. & Sakata, S. Simultaneous electrophysiological recording and fiber photometry in freely behaving mice. *bioRxiv*, 807602 (2019).
57. Bandodkar, A.J. *et al.* Battery-free, skin-interfaced microfluidic/electronic systems for simultaneous electrochemical, colorimetric, and volumetric analysis of sweat. *Science advances* **5**, eaav3294 (2019).

Acknowledgments

The research is supported by National Natural Science Foundation of China (NSFC) (61874064), Beijing Innovation Center for Future Chips, Tsinghua University, and Beijing National Research Center for Information Science and Technology (BNR2019ZS01005). X. S., M. F. and Q. S. are also grateful for the financial support from the CAS Interdisciplinary Innovation Team. We thank L. Sun and Z. Zhou (Peking University), L. Lu and M. Luo (National Institute of Biological Sciences) for valuable discussions. We also thank J. Wei and C. Li (University of Science and Technology Beijing) for the growth of diamond films.

Author contributions:

X. S. developed the concepts. C. L., Y. X., T. W., L. Li, R. L., Y. D., H. D., G. L., G. Z., L. Liu, G. Z., M. F., Q. S., L. Y., and X. S. performed device fabrication and characterization. C. L., C. D., Y. X., and X. S. performed simulations. Y. Z. and X. S. designed circuits. C. L., Y. Z., X. C., Y. X., and X. S. designed and performed biological experiments. C. L. and X. S. wrote the paper in consultation with all other authors.

Competing interests:

The authors declare that they have no competing interests.

Data and materials availability:

All data needed to evaluate the conclusions in the paper are present in the paper and/or the Supplementary Materials. Additional data related to this paper may be requested from the authors.

Figure 1

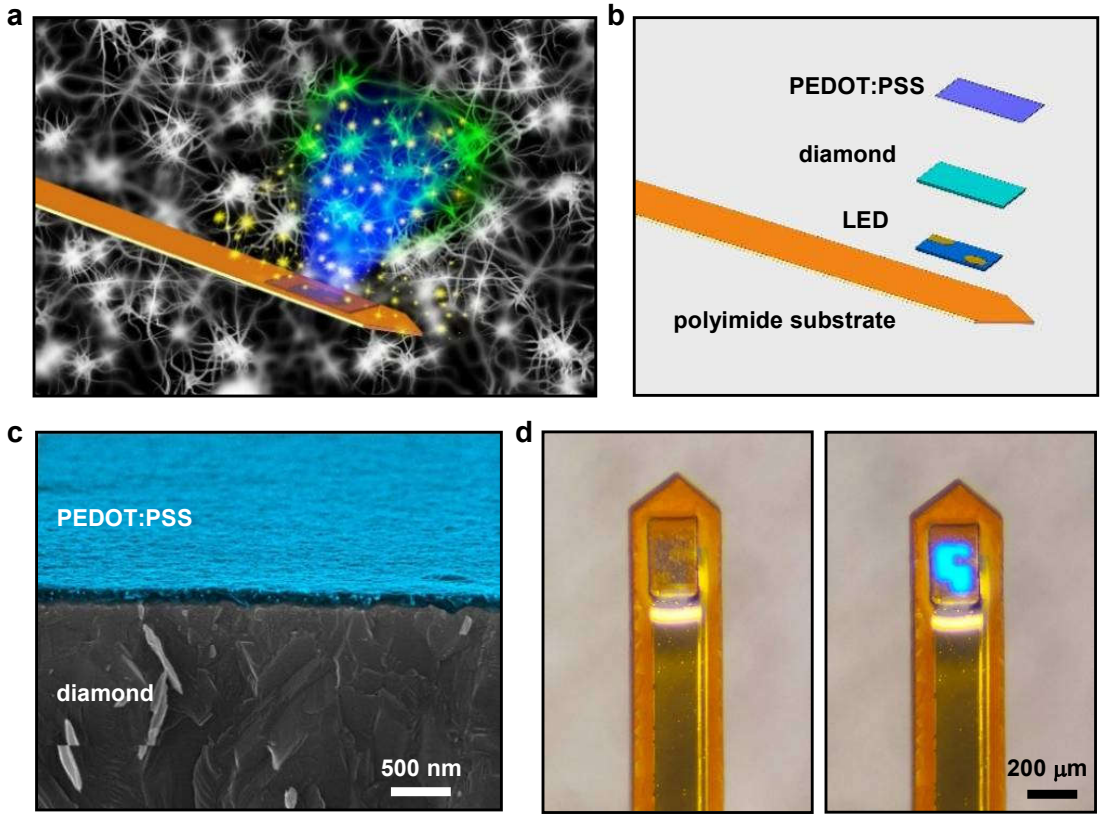

Figure 1. Structures of the implantable microprobe. (a) Conceptual illustration of the microprobe system for optogenetic stimulation and dopamine detection. **(b)** Exploded schematic of the microprobe, comprising a blue micro-LED, a diamond interlayer and a PEDOT:PSS thin film on the PI based substrate. **(c)** Cross-sectional scanning electron microscope (SEM) image of a PEDOT:PSS film (colorized in blue) coated on diamond. **(d)** Optical photographs of a fully fabricated microprobe (left: LED is off; right: LED is on, with an injection current of 0.1 mA).

Figure 2

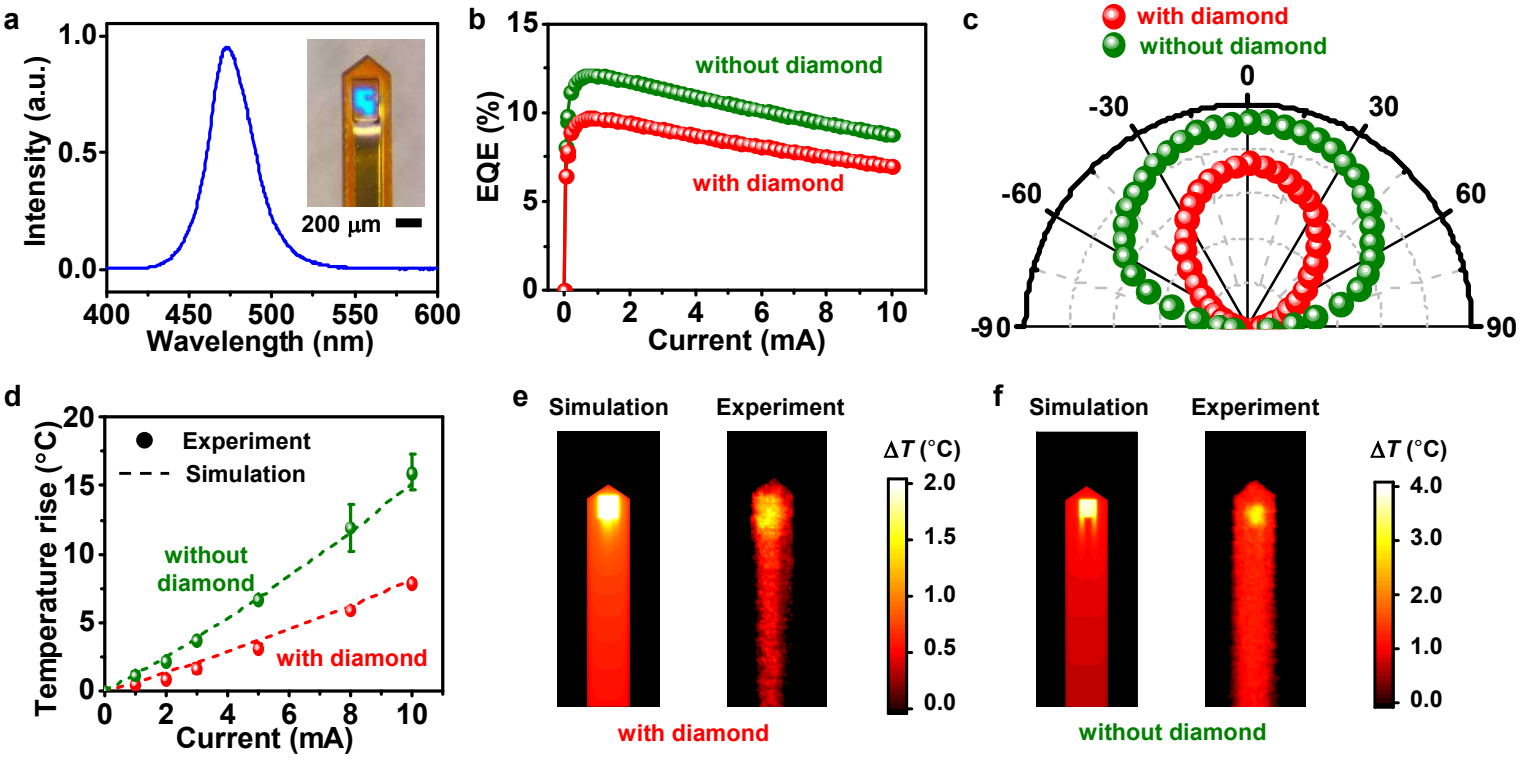

Figure 2. Optoelectronic and thermal characteritics of LEDs in the microprobe. (a) Electroluminescence spectrum of the InGaN blue LED. Inset: optical photograph of the microprobe. **(b)** External quantum efficiencies (EQEs) for LEDs with and without diamond/PEDOT:PSS coatings, under different injection currents. **(c)** Angular distribution of optical emissions for LEDs with and without diamond/PEDOT:PSS coatings. **(d)** Measured (dots) and simulated (dashed lines) maximum temperature rises above room temperature on the top surface of the LED probes (with and without diamond/PEDOT:PSS coatings) as a function of pulsed currents (frequency 20 Hz and duty cycle 20%). **(e, f)** Simulated (left) and measured (right) temperature distributions the LED probes (current 3 mA, frequency 20 Hz and duty cycle 20%), **(e)** with and **(f)** without diamond/PEDOT:PSS coatings.

Figure 3

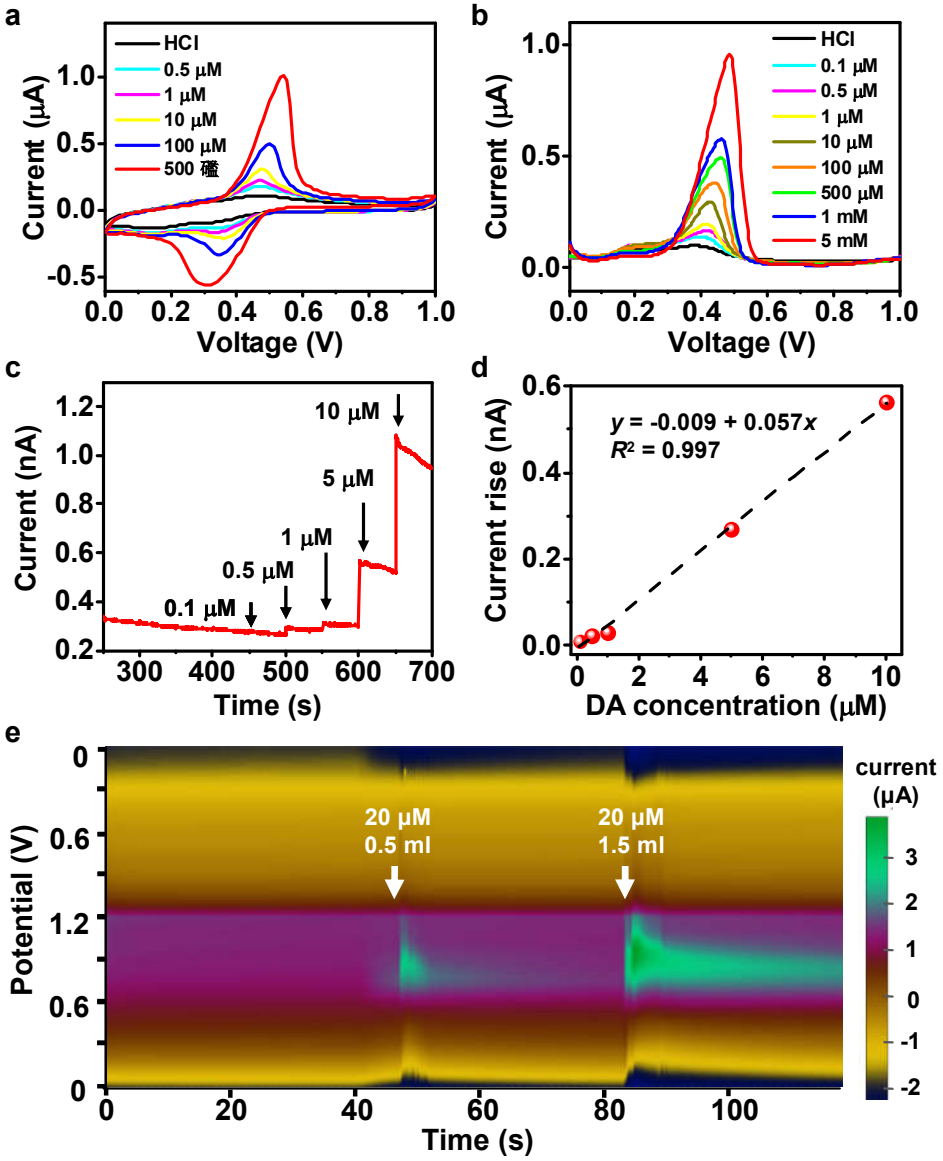

Figure 3. Electrochemical characteristics of the PEDOT:PSS film in the microprobe. (a) Linear sweep voltammetry (LSV). **(b)** Differential pulse voltammetry (DPV). **(c)** Chronoamperometry (CA). **(d)** Calibration curve: linear relationship between response currents and dopamine concentrations (0.1–10 μM). **(e)** Fast scan cyclic voltammetry (FSCV). All the experiments are performed in HCl solutions (pH = 4.0) with varied dopamine concentrations at room temperature, with a saturated Ag/AgCl electrode as the reference and a Pt sheet as the counter electrode.

Figure 4

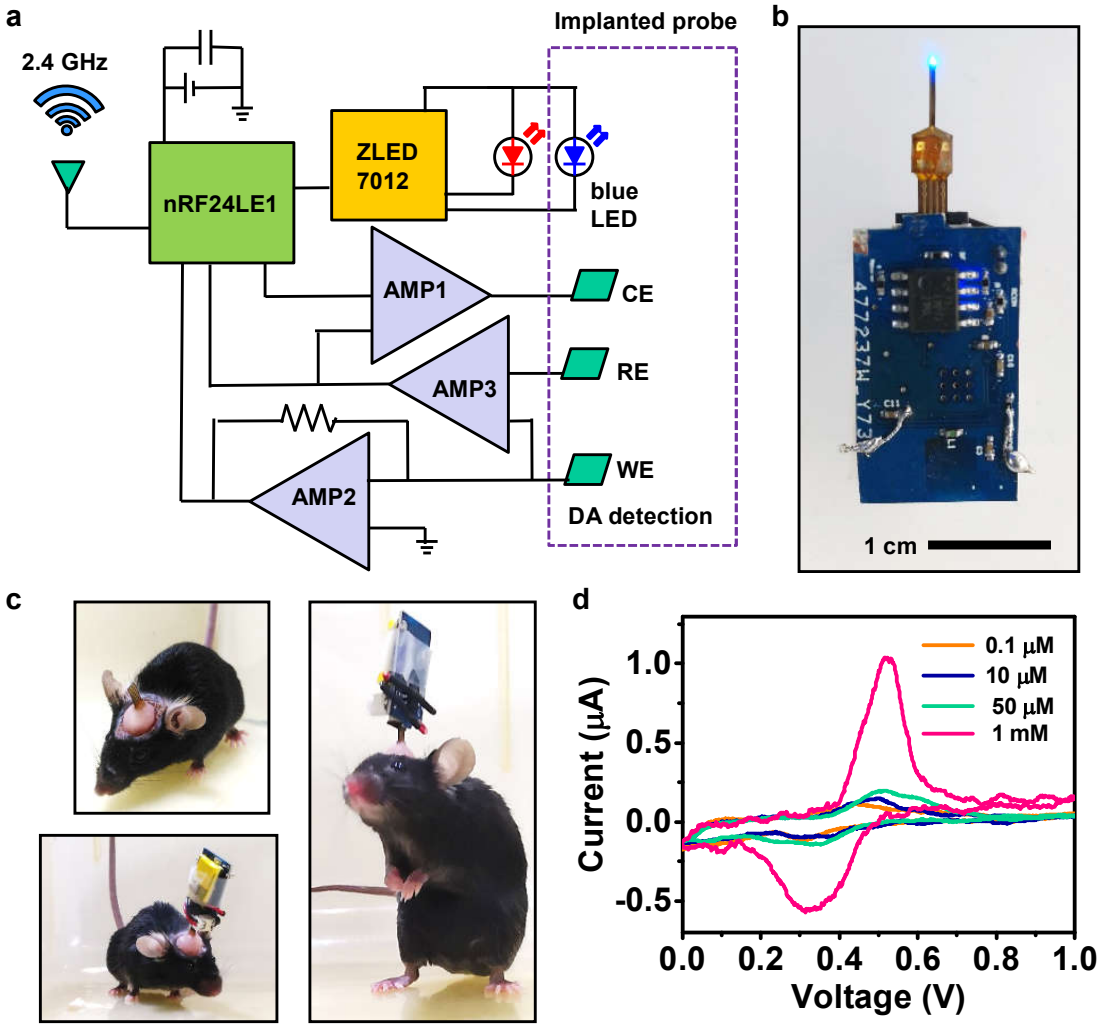

Figure 4. Circuit module for wireless operation. (a) Schematic diagram of the circuit. (b) Photograph of a circuit connected to an implantable probe with the micro-LED on. (c) Photographs of an experimental mouse implanted with the microprobe, with and without the circuit module. (d) LSV curves acquired by the wireless circuit connect to a microprobe in HCl solutions with different dopamine levels.

Figure 5

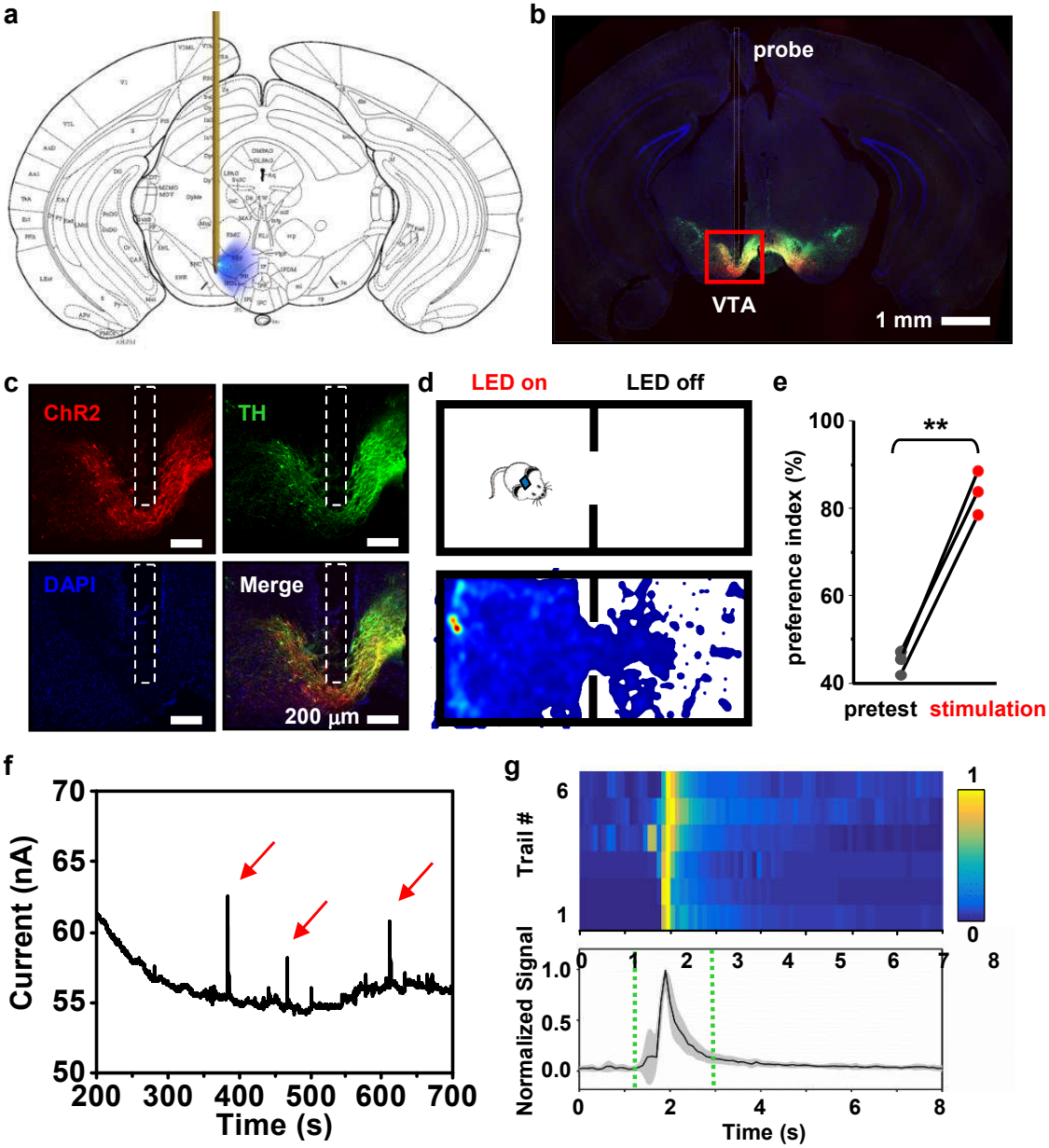

Figure 5. *In vivo* optogenetic stimulation and dopamine detection. (a) Schematic illustration of the mouse brain with the microprobe implanted into the VTA. (b) Immunostained fluorescence image of the brain section. (c) Immunostaining results of the VTA region expressing ChR2 (red), TH (green), DAPI (blue), as well as the merged image. (d) Top: schematica illustration of the real-time place preference (RTPP) tests; bottom: heat map of the animal activity with optogenetic stimulations on the left side of the box. (e) Preference indices on the stimulation side compared to results during pretests (n = 3 mice, $^{**}P < 0.01$). (f) A representative amperometry curve (current versus time) measured with the PEDOT:PSS electrode *in vivo*. (g) Analyses of representative signal peaks. Top: Heatmaps showing 6 individual trials from 3 mice. Bottom: Average of normalized current signals.